

# Matter-wave collimation to picokelvin energies with scattering length and potential shape control

A. Herbst,<sup>1</sup> T. Estrampes,<sup>1,2</sup> H. Albers,<sup>1</sup> R. Corgier,<sup>3</sup> K. Stolzenberg,<sup>1</sup>  
S. Bode,<sup>1</sup> E. Charron,<sup>2</sup> E. M. Rasel,<sup>1</sup> N. Gaaloul,<sup>1</sup> and D. Schlippe<sup>1,\*</sup>

<sup>1</sup>*Leibniz Universität Hannover, Institut für Quantenoptik,*

*Welfengarten 1, 30167 Hannover, Germany*

<sup>2</sup>*Université Paris-Saclay, CNRS, Institut des Sciences Moléculaires d'Orsay, 91405 Orsay, France*

<sup>3</sup>*LNE-SYRTE, Observatoire de Paris, Université PSL, CNRS,*

*Sorbonne Université 61 avenue de l'Observatoire, 75014 Paris, France*

(Dated: October 9, 2023)

We study the impact of atomic interactions on an in-situ collimation method for matter-waves. Building upon an earlier study with  $^{87}\text{Rb}$ , we apply a lensing protocol to  $^{39}\text{K}$  where the atomic scattering length can be tailored by means of magnetic Feshbach resonances. Minimizing interactions, we show an enhancement of the collimation compared to the strong interaction regime, realizing ballistic 2D expansion energies of 438(77) pK in our experiment. Our results are supported by an accurate simulation, describing the ensemble dynamics, which we further use to study the behavior of various trap configurations for different interaction strengths. Based on our findings we propose an advanced scenario which allows for 3D expansion energies below 16 pK by implementing an additional pulsed delta-kick collimation directly after release from the trapping potential. Our results pave the way to achieve state-of-the-art quantum state in typical dipole trap setups required to perform ultra-precise measurements without the need of complex micro-gravity or long baselines environments.

## I. INTRODUCTION

Cooling quantum gases to sub-nanokelvin temperatures has enabled breakthroughs in the fields of quantum sensing [1], quantum information [2] and quantum simulation [3]. Especially in precision sensing and metrology, atom interferometers [4–7] have become a state-of-the-art solution and are used for probing general relativity [8–11], quantum mechanics [12–15], determining fundamental constants [16–18] and measuring inertial effects [19–23]. In these cases, Bose-Einstein condensates (BECs) [24, 25] with expansion energy of a few nanokelvin already offer significant advantages over thermal ensembles with respect to controlling systematic errors and their respective dynamics [26, 27]. However, further collimation into the picokelvin regime is required to achieve the long pulse separation times necessary for future experiments [28–30]. While direct methods such as evaporative cooling [31] and spin gradient cooling [32] allow accessing energies of a few hundred picokelvin, matter-wave lensing [33] is used to reach a few tens of picokelvin in microgravity [34, 35] or long baseline devices [36]. Naturally, these environments are required to enable prolonged free fall times before applying the lens to enter the ballistic regime and minimize atomic interactions, which would otherwise drive the expansion post-lensing [36, 37].

Here we demonstrate a novel approach to resolve this issue by use of a Feshbach resonance [38, 39] to tailor interactions during the lens and upon release from the trapping potential. Using a  $^{39}\text{K}$  BEC in the weak interaction regime, we achieve expansion energies below

500 pK in two dimensions, which is a substantial improvement over previous results achieved with the same method and setup using  $^{87}\text{Rb}$  [40]. Furthermore, our systematic analysis reveals that the careful adjustment of trapping frequencies and interactions will allow to reach 3D expansion energies below 16 pK, when implementing an additional delta-kick collimation (DKC) pulse [33] after a few milliseconds of free fall. Hence, our method allows for state-of-the-art collimation in typical or even compact quantum optics experiments, without excessive hardware or environmental requirements.

## II. RESULTS

We apply the matter-wave lensing protocol as described in reference [40]. Using a center-position modulation (CPM) of the trapping beams, created with an acousto-optical modulator (AOM), we realize time-averaged optical potentials [41] of harmonic shape with variable width and depth in the horizontal  $\{x, y\}$ -plane (c.f. section IV A). Here the  $\{x, y, z\}$ -coordinates refer to the trap frame which is also used to specify all following trap frequencies. By rapidly relaxing the trap within 50  $\mu\text{s}$  we cause a sudden reduction in trap frequencies from initial frequencies  $\omega_i^I$  to final frequencies  $\omega_i^F < \omega_i^I$  for  $i \in \{x, y\}$ , inducing collective mode excitations [42, 43]. Subsequently, the ensemble is collimated by turning off the trapping potential at the turning point of the resulting size oscillation. We apply this method at two different scattering lengths  $158 \text{ a}_0$  and  $10 \text{ a}_0$  at which the interaction and kinetic energy terms respectively dominate (c.f. section IV D). In the following we differentiate between expansion energies along a singular axis in  $i$ -

\* Email: schlippe@iqo.uni-hannover.de

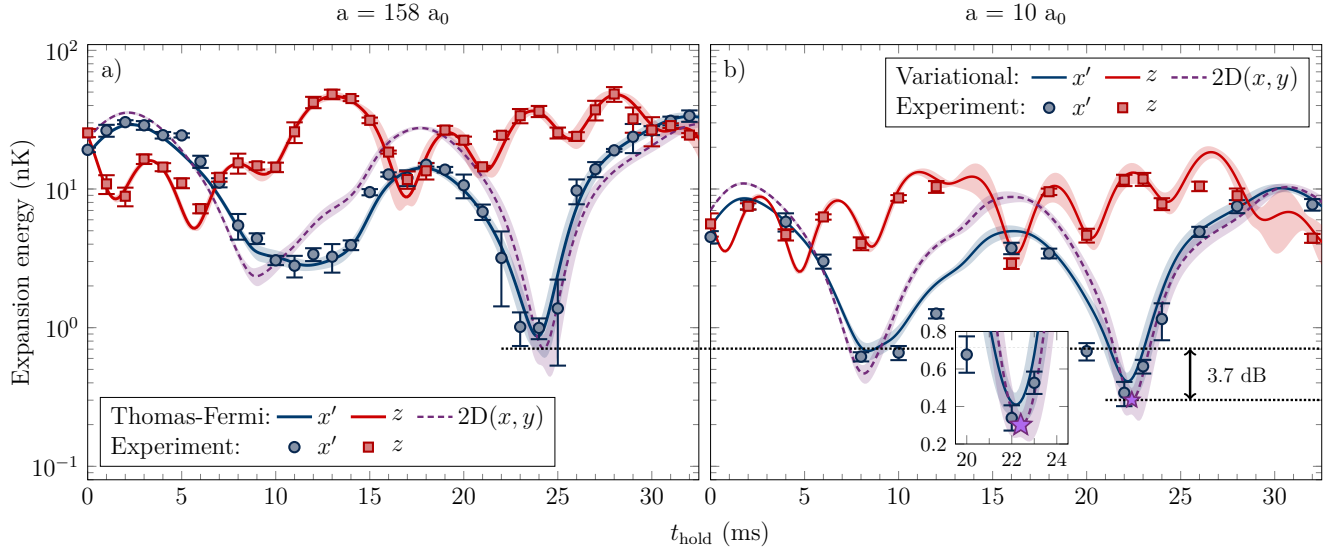


FIG. 1. **Measured and simulated 1D expansion energy  $E^{1D}$  for  $158 a_0$  (a) and  $10 a_0$  (b) scattering length in the camera frame and 2D expansion energies  $E^{2D}$  in the horizontal plane.** For each measurement (points) the error bars are obtained from the fit uncertainty of the expansion in the individual TOF series (c.f. section IV C). For the  $10 a_0$  case we choose a lower sampling rate, allowing to increase the number of points per TOF measurement in order to resolve the lower expansion energies, effectively. The dynamics of the ensemble are simulated (lines) based on the Thomas-Fermi approximation for  $158 a_0$ , while at  $10 a_0$  a variational approach is used (c.f. section IV D). In both cases the shown simulations correspond to a TOF of 25 ms and are limited by the maximum observable time during the experiment. Uncertainty bands are obtained by a Monte Carlo method based on the detection angle and trap frequency errors matching the behavior of the size oscillations. The measurements agree well with the simulation, and we extrapolate an overall improvement by 3.7 dB in 2D expansion energy, as shown by the purple dashed lines, when reducing the scattering length. The purple star highlights the minimum 2D energy at  $10 a_0$ , as prominently featured in the inset

direction ( $E_i^{1D}$ ), 2D energies in the horizontal plane in which the lensing takes place ( $E^{2D}$ ) and the full three dimensional expansion energy ( $E^{3D}$ ). For both measurements at the two different scattering lengths, we use the same initial and final trap configurations, with small variations of the parameters resulting only from pointing instabilities of the optical dipole trap (ODT) beams which we relate to the time passed between the two measurement campaigns. In both cases the initial trap is realized without any CPM. We find initial trapping frequencies of  $2\pi \times \{72, 144, 115\}$  Hz for  $158 a_0$  and  $2\pi \times \{62, 149, 96\}$  Hz for  $10 a_0$ . After relaxation our final trap frequencies are  $2\pi \times \{23, 36, 126\}$  Hz for  $158 a_0$  and  $2\pi \times \{24, 38, 129\}$  Hz for  $10 a_0$ . In parallel the trap depth is maintained by increasing the laser intensity, suppressing atom number loss. Based on time-of-flight (TOF) measurements of the ensemble's expansion, we determine the expansion energies along the horizontal (collimated)  $x'$ - and vertical (not collimated)  $z$ -direction within the camera frame  $\{x', y', z\}$  (c.f. section IV A) for different holding times  $t_{\text{hold}}$ , after relaxing the trap. At a scattering length of  $158 a_0$  (Fig. 1a) the minimal value in the collimated direction yields  $E_{x'}^{1D} = 1.00(17)$  nK and is achieved after a holding time of 24 ms. For  $10 a_0$  (Fig. 1b) we find the minimum for a holding time of 22 ms after decompression. While analyzing the expansion velocities results in

a minimal value of  $E_{x'}^{1D} = 340(12)$  pK after up to 25 ms TOF, the ensemble has not yet reached the linear expansion regime at that point. Simulating the behavior (c.f. section IV C) agrees with these findings, however the same simulation performed in the ballistic regime for a TOF of 250 ms yields an minimum of  $E_{x'}^{1D} = 429(56)$  pK after 22.1 ms.

The excellent agreement between experiment and simulation allows to understand the ensemble's dynamics in the entire horizontal plane and to include the axis which cannot be directly observed due to the camera orientation. The determined 2D expansion energies is depicted as dashed purple lines in Fig 1. At  $10 a_0$  we find a minimal value of  $E^{2D} = 438(77)$  pK [resp.  $301(65)$  pK] for a TOF of 250 ms [resp. 25 ms], which corresponds to an improvement by 3.7 dB over the  $158 a_0$  case.

### III. DISCUSSION

#### A. Comparison to previous results

In this work we applied our matter-wave collimation protocol previously developed for  $^{87}\text{Rb}$  to a  $^{39}\text{K}$  BEC and prove the ease of application to another atomic species, demonstrating an improvement by 13 dB over the non-

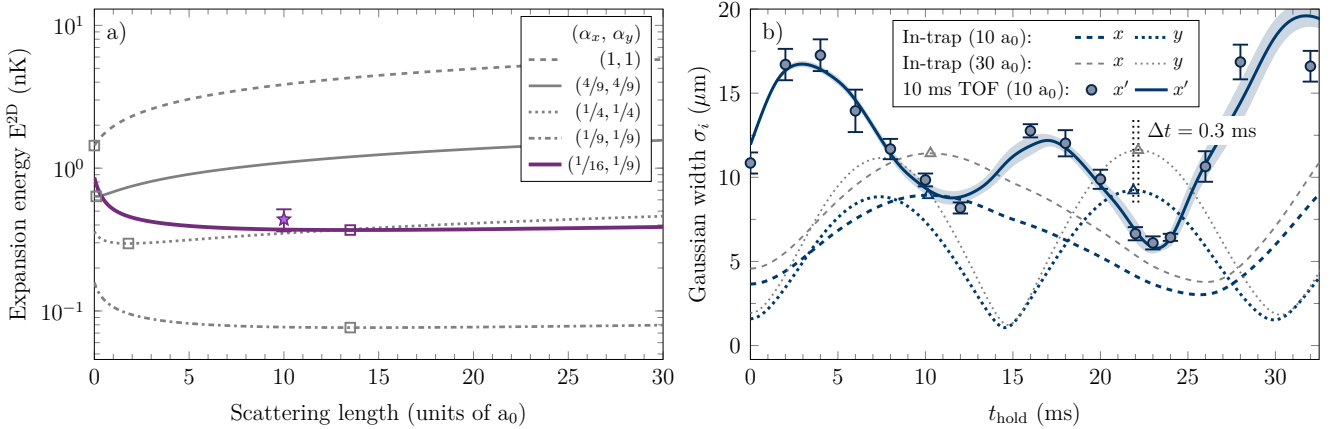


FIG. 2. (a) Simulated 2D expansion energy  $E^{2D}$  in the collimated plane for different scaling factors  $\alpha_i$  and for the configuration used in the experiment (see section II) after 25 ms TOF. (b) Measured ensemble width in  $x'$ -direction for 10 ms TOF at 10  $a_0$  and corresponding size oscillations in  $x$ - and  $y$ -direction within the trapping potential, as simulated for 10  $a_0$  and 30  $a_0$ . For a common frequency reduction along both lensed directions with  $\alpha_x = \alpha_y$  taking respectively the values  $\{1, 4/9, 1/4, 1/9\}$ , the minimal energies are obtained for a scattering length  $a$  being respectively  $\{0, 0.1, 1.8, 13.5\} a_0$  and identified by the squares for each case. Here, the simulation are performed for a fixed set of parameters. The purple star resembles the lowest 2D experimental expansion energy presented in Fig. 1b (obtained here for 250 ms TOF). This point is obtained within a Monte-Carlo simulation including all experimental uncertainties. The error bar denotes  $2\sigma$  deviation while the central point stands for the mean value (see section IV C). Since  $\alpha_x \approx 1/16$  and  $\alpha_y \approx 1/9$  for the experimental configuration the optimal release points differ for each axis as highlighted by the triangle symbols. Additionally, changing the scattering length from 10  $a_0$  to 30  $a_0$  shifts the optimal release time by  $\Delta t = 0.3$  ms.

collimated case, as given for vanishing holding time. Considering the mass ratio of both elements our results for  $^{39}\text{K}$  at 158  $a_0$  are comparable to the previously achieved result of 3.2(6) nK with  $^{87}\text{Rb}$  [40] at its natural background scattering length of  $\sim 100 a_0$  [44]. This result is expected since the technique only depends on the ensemble's dynamic as governed by interactions and trap frequencies and described through the Gross-Pitaevskii equation. More importantly, we show that the final expansion energy after the lens can be further reduced by minimizing the scattering length, as done here by means of a magnetic Feshbach resonance. By reducing the repulsive forces driving the expansion after release from the trap, we achieve expansion energies well below 1 nK, which is necessary to match the requirements of proposed experiments, e.g. for, but not limited to, gravitational wave detection [45–50], test of the Weak Equivalence Principle [8, 11, 51] or the search for dark matter [52–54]. While the energies realized here are still an order of magnitude larger than in previous demonstrations in two [36] and three dimensions [34], our method can be applied directly in the ODT. Hence it is suitable for setups and applications which do not allow for an extended pre-expansion time before applying the lens due to constraints regarding experimental cycle time or spatial dimensions. Lower expansion energies are currently limited by the achievable maximum CPM amplitude of 200  $\mu\text{m}$  which in turn restricts the range of accessible trapping frequencies to the values given in section II.

## B. Scattering length and trap frequency dependencies

To gain insight into the impact of the scattering length onto the collimation, we analyze the ensemble's behavior in the weak interaction regime by simulating the dynamics with an adapted theoretical model for two different scenarios (Fig. 2a). Starting from trap frequencies of  $2\pi \times 60$  Hz in all directions, we apply a common reduction in the horizontal plane while maintaining the frequency along the  $z$ -axis, as shown by the theoretical grey lines. For all scenarios we evaluate the optimal holding time after relaxing the trap for minimizing  $E^{2D}$  and study the behavior for different squared trap frequency ratios  $\alpha_i = (\omega_i^F/\omega_i^I)^2$ , which would provide the energy scaling in the ideal gas regime [55]. As previously discussed in reference [36] and also observed here, the energy reduction for a BEC is significantly higher due to an interplay of interactions and coupling of the size oscillations along each axis. From the theory simulations we find a reduction of the expansion energy towards smaller scattering length for  $\alpha_x = \alpha_y > 4/9$  as shown by the dashed grey line. This result matches the expected dynamics of an ensemble during free-fall expansion without any lensing and is explained by repulsive interactions after removing the trapping potential [56–58]. Interestingly, we identify a minimal expansion energy at non-zero interactions for  $\alpha_x = \alpha_y \lesssim 4/9$ , as depicted by the continuous, dotted and dash-dotted grey lines. These curves clearly show that for smaller values of  $\alpha_i$ , reaching optimal energies

requires to move towards higher scattering length values. Regarding the experimental setup, as shown by the purple line, where the change in aspect ratio is not the same for both directions,  $\alpha_x \approx 1/16$  and  $\alpha_y \approx 1/9$ , we find back the same behavior as described above for the case  $\alpha_x = \alpha_y \lesssim 4/9$ . This can be explained by the fact that  $\sqrt{\alpha_x \alpha_y} = 1/12$ . Note here that the purple star is identical to the one already shown in Fig. 1b.

To get further insight of the complex behavior of the matter-wave for different scattering length we now compare in Fig 2b scenarios at  $a = 10 a_0$  (blue thick lines) and  $30 a_0$  (grey thin lines). There we show the two directions in the trap,  $x$  in dashed and  $y$  in dotted. As expected larger interaction strength lead to larger oscillation amplitudes. To achieve a minimum momentum spread in free fall one hence wants to increase the interactions during the lens to maximize the cloud size and cancel them at the release time. However, given that the interactions are controlled via magnetic fields such an optimization is technically not feasible, as it typically takes tens of millisecond to change the magnetic field [39]. Therefore the optimal scattering length has to be found as a trade-off between the maximum size achievable within the trap and minimal repulsive interactions in free fall along the horizontal direction. Such optimized configurations are highlighted by the empty squares in Fig. 2a.

For the configuration  $a = 10 a_0$ , the experimental measurements of the widths after 10 ms TOF show two distinct minima which are connected to the maxima of the underlying size oscillations within the trap (blue circles). These minima are caused by the different aspect ratio along the two directions shown by the blue dashed and dotted line for the  $x$ - and  $y$ -direction respectively and where the local maximum is depicted by the empty triangle. In this specific case the lowest expansion energy  $E^{2D}$  is found near the optimal collimation of the  $y$ -direction, closely resembling the case  $\alpha_x = \alpha_y = 1/9$  in Fig. 2a but with globally higher energies caused by the expansion in the  $x$ -direction. Comparing to a similar configuration with  $a = 30 a_0$ , one note that the optimal release timing is extremely robust with respect to imperfect control of the Feshbach field, giving only 0.3 ms offset.

Overall, our analysis yields the choice of trapping frequencies to be more important due to their enhanced scaling than the exact scattering length knowledge which are more difficult to pinpoint in practice. Besides allowing to extract the 2D expansion energy from the measurements, the adequacy between the experiment and theory model in Fig. 1 and Fig. 2 allow us in the following to identify advanced collimation scenarios. Consecutively, we discuss two 3D collimation sequences based on the combination of a 2D in-trapped collimation combined with a pulse delta-kick method collimating the third axis to reach the pK regime [34, 59].

### C. Advanced Scenario

Since neither the demonstrated method, nor the experimental apparatus is designed to collimate the remaining vertical axis, the achievable 3D expansion energies are limited to the nanokelvin regime, regardless of the performance in the horizontal plane, as shown by the horizontal dashed line in Fig. 3a. To overcome this limitation we consider a short TOF after the end of the holding process followed by a pulsed DKC protocol [33–36]. We study the theoretically achievable expansion energies for this sequence in an advanced scenario which is specifically tailored towards the capabilities of the improved apparatus as presented in reference [61] and highlight the crucial requirements for the implementation. Instead of a recycled ODT, the setup features two individually controllable beams, each with up to 16 W of optical power at a wavelength of 1064 nm. This configuration allows to realize a variety of possible trap geometries and especially to design common turning points for the size oscillations along both principal axes. Furthermore, 2D acousto-optical deflectors (AODs) [*AA Opto-Electronic DTSXY-400-1064*] are used to create time-averaged optical potentials instead of the previously used AOM. In combination with the implemented lens-system, their superior bandwidth allows for CPM amplitudes of at least 1.5 mm and consequently to access lower final trap frequencies and expansion energies. Finally, for the DKC, the second AOD axis is needed to shift the ODT beams vertically and match the position of the atomic cloud for a maximum TOF of 25 ms, corresponding to a free-fall distance of 3 mm.

For  $E^{2D}$  we numerically find minimal values below 20 pK for a holding time of 42.5 ms switching the trap frequencies from  $2\pi \times \{152.7, 310.7, 342.6\}$  Hz to  $2\pi \times \{28.1, 5.6, 340.0\}$  Hz at  $10 a_0$  scattering length (c.f. Fig. 3a). For the final trap configuration 150 mW of optical power at a CPM amplitude of 175  $\mu\text{m}$  for one and 450 mW with 800  $\mu\text{m}$  modulation stroke for the other beam is required. Indeed, as the frequency along the vertical axis is much higher than the two others, the DKC will not significantly affect the other direction as shown by the dotted curves in Fig. 3b. For an easy configuration with only 10 ms TOF, corresponding to a free fall distance of 490  $\mu\text{m}$ , experimentally accessible in practice, we obtain a minimal 3D expansion energy of  $E^{3D} = 24.5$  pK with a  $\delta t_{\text{DKC}} = 18.8$   $\mu\text{s}$  long delta-kick pulse and 44.8 ms of lensing as shown in Fig. 3c. Moreover, the implementation is expected to be robust against variations of the experimental parameters as it allows to achieve energies below 50 pK for a wide range of holding and delta-kick durations. Naturally, even better performance can be obtained by increasing the TOF duration at the expense of the overall robustness with respect to the delta-kick timing [33]. For 25 ms of TOF, we find final energies as low as  $E^{3D} = 15.7$  pK, but requiring a DKC of only  $\delta t_{\text{DKC}} = 6.2$   $\mu\text{s}$  (Fig. 3d). While this simulation already takes the response time of the AOD into account,

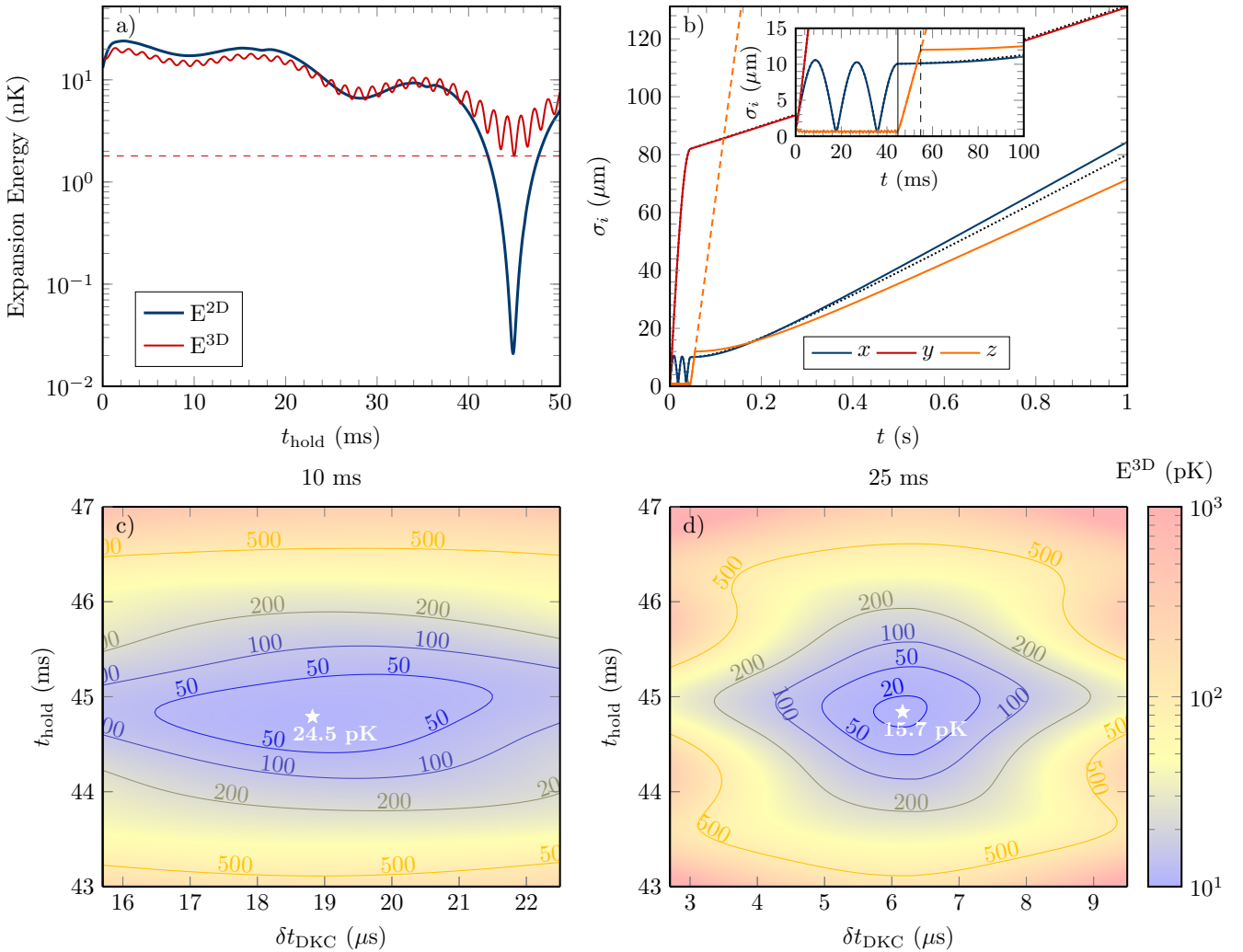


FIG. 3. (a) Expansion energy taking advantage only of the holding process, after trap relaxation. (b) Width evolution in all three directions after the optimal holding period without (dotted lines) and with a DKC (solid lines). The inset shows the dynamics in the trapping potential, highlighting release and DKC timings. (c,d) 3D expansion temperature as a function of the lensing time and the DKC duration after a TOF of respectively 10 ms and 25 ms. While an optimal release timing allows for 2D energies in the two-digit picokelvin range, the total energy in three dimensions is limited by the vertical  $z$ -axis shown by the orange dashed line. Applying an additional pulsed delta-kick (black dashed line) allows to reduce the expansion of the vertical axis as well, while only marginally affecting the other two, shown in dotted lines, due to large differences in the trap frequencies. Using a simulated annealing algorithm [60], we optimized the lensing and DKC duration to reach 24.5 pK and 15.7 pK in the case of  $10 a_0$  scattering length.

such timings can nevertheless be experimentally challenging when being limited to the center-position modulation frequency below 100 kHz as relevant time scale. For this apparatus we use a software defined radio [*Ettus USRP X310*] as rf-driver, which allows to interrupt the waveform at any given sample and match the pulse length with a resolution of 50 ns for a typical sampling rate of 20 MHz. As before using a low scattering length assists in the overall collimation. However, simulating the same sequence for a scattering length of  $158 a_0$  in particular, still leads to expansion energies of  $E^{3\text{D}} = 97.5 \text{ pK}$  for 10 ms of TOF and  $E^{3\text{D}} = 81.9 \text{ pK}$  for 25 ms with  $17.6 \mu\text{s}$

and  $7.1 \mu\text{s}$  long delta-kick pulses, respectively.

Hence, the analyzed two-step process opens up the path to approach ( $a = 158 a_0$ ) and even exceed ( $a = 10 a_0$ ) the results that were obtained in a drop-tower [34], on the International Space Station [35] and within a long baseline device [36]. Combining these results with a strategy for rapid evaporation [61] and a bright source for fast MOT loading [62], compact or even fieldable devices can reach experimental repetition rates higher than 0.5 Hz with BECs consisting of  $3 \times 10^5$  atoms and state-of-the-art collimation.

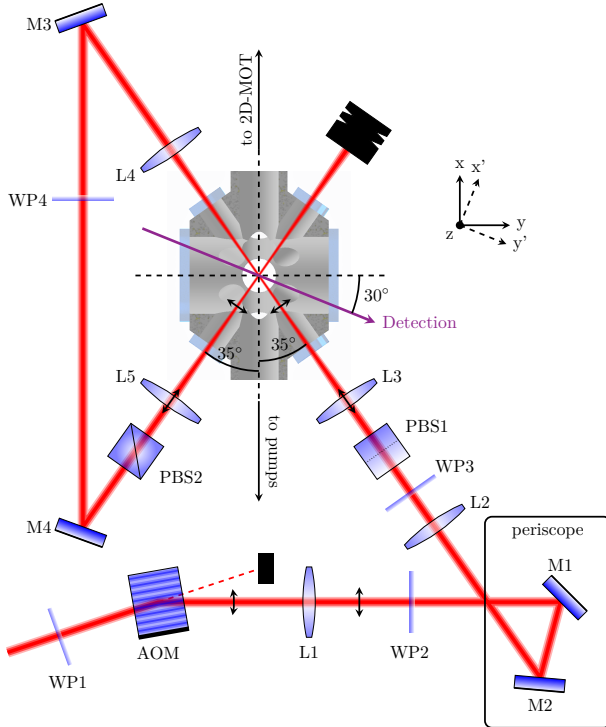


FIG. 4. **Experimental apparatus to create the optical dipole trap and the matter-wave lens.** A three-lens system ( $L_1$ ,  $L_2$ ,  $L_3$ ) with focal lengths  $f_1 = 100$  mm,  $f_2 = 300$  mm and  $f_3 = 150$  mm translates the change in AOM deflection angle into a parallel displacement, while simultaneously focusing the beam to a waist of 30 (45)  $\mu\text{m}$  in horizontal (vertical) direction. Orthogonal polarization between the crossing beams is realized by a combination of  $\lambda/2$ -wave plates (WP3 and WP4) and polarizing beam splitters (PBS1 and PBS2). For perfect alignment and equal beam power the trap frame  $\{x, y, z\}$ , as given by the principal axes of the optical potential, resembles the symmetry axes of the vacuum chamber. The camera frame  $\{x', y', z\}$  is obtained by a rotation around the  $z$ -axis, with the exact detection angle depending on the beam configuration and alignment. The figure is taken from reference [40] and was published under Creative Commons Attribution 4.0 International License. Here the orientation of the detection arrow and the naming of the coordinate systems was altered to account for changes of the apparatus compared to the source material.

#### IV. METHODS

##### A. Experimental apparatus

We use the same setup as for the previous matter-wave lens study with  $^{87}\text{Rb}$  [40], featuring a crossed ODT in recycled beam configuration (Fig. 4). A detailed description of the vacuum, laser and coil systems used can be found in references [8, 10, 63]. The ODT is based on a 1960 nm fiber laser [IPG TLR-50-1960-LP] which is intensity stabilized by a feedback loop, controlling a linearized Pockels cell. A custom-made AOM [Polytec

ATM-1002FA53.24] is used to implement time-averaged optical potentials of harmonic shape along one beam axis [41, 64]. It is further utilized to control the beam power at the lower end of the intensity stabilization. By focusing the beam onto the atomic cloud, the change in deflection angle of the AOM is translated into a parallel displacement of the beam. Thereby, the required frequency modulation of the rf-signal driving the AOM is generated with a combination of voltage controlled oscillator [Mini-Circuits ZOS-150+] to provide the actual signal and an arbitrary waveform generator [Rigol DG1022Z], which provides the waveform. For the whole experimental sequence a constant modulation frequency of 20 kHz is used, which is sufficiently large compared to any occurring trap frequency. The crossed trap is realized by re-cycling the same beam, passing the atoms again under an angle of 70°. We ensure orthogonal beam polarization to avoid running lattice formation. Due to the elliptical beam shape of the fiber laser output we obtain different beam waists of 30  $\mu\text{m}$  in horizontal and 45  $\mu\text{m}$  in vertical direction. Taking losses at all optical elements into account, the maximal power which can be delivered to the atoms is limited to 8 W for the initial and 6 W for the recycled beam, while the bandwidth of the AOM allows for a maximum CPM amplitude of 200  $\mu\text{m}$  and 300  $\mu\text{m}$ , respectively.

Finally, detection is performed by absorption imaging with one to one mapping. The camera is situated in the  $\{x, y\}$ -plane and the related camera frame  $\{x', y', z\}$  can be obtained from the trap frame  $\{x, y, z\}$  by rotating clockwise around the  $z$ -axis with an angle of  $\sim 30^\circ$  with respect to the  $y$ -axis.

##### B. Ensemble preparation

We apply a trap loading and state preparation sequence optimized for  $^{39}\text{K}$  as described in reference [63]. We load a 3D-magneto optical trap on the  $\text{D}_2$ -line from a 2D-MOT, trapping  $1 \times 10^9$  atoms within 4 s. Subsequently, we apply a hybrid  $\text{D}_1$ - $\text{D}_2$  compression MOT to increase the ensemble's density and grey molasses cooling on the  $\text{D}_1$ -line for cooling the ensemble to sub-Doppler temperatures [65]. In this manner we prepare  $4 \times 10^8$  atoms at a temperature of 12  $\mu\text{K}$  within 56 ms after turning off the 2D-MOT. For loading the ODT we use a center-position modulation amplitude of 160  $\mu\text{m}$  to improve the mode matching of the crossing region with the cloud, transferring  $12 \times 10^6$  atoms into the 54  $\mu\text{K}$  deep ODT, with a temperature of 8.5  $\mu\text{K}$ . Afterwards, we prepare the ensemble in  $|F = 1, m_F = -1\rangle$  with a multi-loop state preparation scheme based on microwave adiabatic rapid passages. This allows to use the broad Feshbach resonance at 32.6 G [66] to adjust the scattering length to positive values, necessary for direct evaporative cooling [67]. We use the evaporation sequence optimized for the largest number of condensed particle, rather than the shortest experimental cycle time with the highest atomic

flux, realizing a quasi-pure BEC of up to  $2 \times 10^5$  atoms after 3.9 s of evaporative cooling at a scattering length of  $158 \text{ a}_0$ . For the measurement at  $158 \text{ a}_0$  we perform the matter-wave lens 100 ms after creating the BEC by increasing the center-position modulation amplitude to the achievable maximum of 200  $\mu\text{m}$ . For the measurement at  $10 \text{ a}_0$ , we additionally adiabatically sweep the magnetic field towards the broad minimum between the resonance at 32.6 G and the next higher one at 162.8 G after creating the BEC and before performing the matter-wave lens.

### C. Data acquisition and analysis

We perform TOF measurements for different holding times after relaxing the trap with a total experimental cycle time of 12 s. Subsequently we describe the obtained density profile either by a Gaussian or a Thomas-Fermi distribution, depending on the scattering length used. For the measurements at  $158 \text{ a}_0$  the Thomas-Fermi radii  $R_i(t)$  are transformed into their equivalent Gaussian standard deviation  $\sigma_i(t)$  using  $\sigma_i(t) = R_i(t)/\sqrt{7}$  [59, 68]. Individual data points are taken for a holding time spacing of 1 ms and a TOF spacing of 5 ms. Each measurement is repeated at least four times. At  $10 \text{ a}_0$  we fit a Gaussian to the obtained density distribution. For these measurements the TOF spacing is reduced to 1 ms at the expense of the holding time spacing which is increased to at least 2 ms, in order to obtain better statistics for the extracted ensemble expansion. The total amount of data taken is limited by the available time of continuous operation of the apparatus in order to ensure comparability within a single dataset. To obtain the linear expansion rate for a given holding time, we only consider the data taken for more than 10 ms TOF, avoiding the resolution limitation of our detection system. Finally, the fitted expansion rates  $v_i$  are transformed into 1D expansion energy using  $E_i^{\text{1D}} = k_B T_i/2 = mv_i^2/2$ .

To simulate the behavior of the ensemble, we determine the trapping frequencies by fitting the size oscillations with respect to the holding time for a constant TOF in the trap frame and by projecting them into the rotated camera frame, afterwards. Since the detection angle relative to the trap frame changes with respect to small deviations of the ODT beam alignment, the exact angle is evaluated for each measurement separately and fitted to the data, as well. We optimize the fit parameters on five different TOF in between 10 and 25 ms simultaneously with equal weighting, obtaining a single set of values, which provide the overall smallest error. Based on the frequencies found, we perform simulations of the ensemble's behavior using the two approaches provided in section IV D. The error bands stem from 1000 Monte-Carlo simulations within the obtained errors of trap frequencies, detection angle and scattering length (at  $10 \text{ a}_0$ ) as determined by fitting the size oscillations

and the magnetic field characterization of the apparatus.

For the advanced scenario we take experimental parameters and technical limitations of the setup, e.g. the rise time of the AOD, into account. We search for optimal 3D collimation by simulating a grid with a step size of 36  $\mu\text{s}$  for the lensing and 62 ns for the DKC, using a simulated annealing algorithm [60] for the absolute minimum in each case.

### D. Theoretical model

For a scattering length of  $158 \text{ a}_0$ , the interaction energy exceeds the kinetic energy of the ensemble, so the BEC dynamics is well described by the scaling equations of Refs. [69, 70]

$$\ddot{\lambda}_i(t) + \omega_i^2(t)\lambda_i(t) = \frac{\omega_i^2(0)}{\lambda_i \lambda_x \lambda_y \lambda_z}, \quad (1)$$

where the dimensionless variable  $\lambda_i(t) = R_i(t)/R_i(0)$  characterizes the evolution of the size of the condensate in the direction  $i \in \{x, y, z\}$ . In this expression,  $R_i(t)$  is the Thomas-Fermi radius in the direction  $i$ , and the initial radius is given by [71]

$$R_i(0) = a_{\text{osc}} \frac{\bar{\omega}(0)}{\omega_i(0)} \left( \frac{15Na}{a_{\text{osc}}} \right)^{1/5}, \quad (2)$$

with the average length of the quantum harmonic oscillator  $a_{\text{osc}} = [\hbar/m\bar{\omega}(0)]^{1/2}$  and the geometric mean of the initial trapping frequencies  $\bar{\omega}(0) = [\omega_x(0)\omega_y(0)\omega_z(0)]^{1/3}$ . From the solution of Eq. (1) we extract the standard deviations  $\sigma_i(t) = R_i(t)/\sqrt{7}$  associated with the atomic density, that we compare with the experimental measurements obtained as described in section IV C.

In the case of a scattering length of  $10 \text{ a}_0$ , the Thomas-Fermi approximation is no longer suitable to accurately describe the dynamics of the BEC. Instead, we follow a variational approach and describe the BEC with a Gaussian ansatz [72, 73]. This leads in a harmonic trap to the following set of coupled differential equations

$$\ddot{\sigma}_i(t) + \omega_i^2(t)\sigma_i(t) = \frac{\hbar^2}{4m^2\sigma_i^3(t)} + \frac{\hbar^2aN}{4\sqrt{\pi}m^2} \frac{1}{\sigma_i\sigma_x\sigma_y\sigma_z}, \quad (3)$$

for the standard deviations  $\sigma_i(t)$  of the atomic density. The time-independent version of Eq. (3) is used to determine the initial size  $\sigma_i(0)$  of the ensemble, which converges to the oscillator length for vanishing scattering length.

## DATA AVAILABILITY

The data used in this manuscript is available from the corresponding author upon reasonable request.

---

[1] C. L. Degen, F. Reinhard, and P. Cappellaro, Quantum sensing, *Rev. Mod. Phys.* **89**, 035002 (2017).

[2] O. Mandel, M. Greiner, A. Widera, T. Rom, T. W. Hänsch, and I. Bloch, Controlled collisions for multi-particle entanglement of optically trapped atoms, *Nature* **425**, 937 (2003).

[3] I. M. Georgescu, S. Ashhab, and F. Nori, Quantum simulation, *Rev. Mod. Phys.* **86**, 153 (2014).

[4] M. Kasevich and S. Chu, Atomic interferometry using stimulated raman transitions, *Phys. Rev. Lett.* **67**, 181 (1991).

[5] M. Kasevich and S. Chu, Measurement of the gravitational acceleration of an atom with a light-pulse atom interferometer, *Applied Physics B* **54**, 321 (1992).

[6] F. Riehle, T. Kisters, A. Witte, J. Helmcke, and C. J. Bordé, Optical ramsey spectroscopy in a rotating frame: Sagnac effect in a matter-wave interferometer, *Phys. Rev. Lett.* **67**, 177 (1991).

[7] A. D. Cronin, J. Schmiedmayer, and D. E. Pritchard, Optics and interferometry with atoms and molecules, *Rev. Mod. Phys.* **81**, 1051 (2009).

[8] D. Schlippert, J. Hartwig, H. Albers, L. L. Richardson, C. Schubert, A. Roura, W. P. Schleich, W. Ertmer, and E. M. Rasel, Quantum test of the universality of free fall, *Phys. Rev. Lett.* **112**, 203002 (2014).

[9] M. G. Tarallo, T. Mazzoni, N. Poli, D. V. Sutyrin, X. Zhang, and G. M. Tino, Test of einstein equivalence principle for 0-spin and half-integer-spin atoms: Search for spin-gravity coupling effects, *Phys. Rev. Lett.* **113**, 023005 (2014).

[10] H. Albers, A. Herbst, L. L. Richardson, H. Heine, D. Nath, J. Hartwig, C. Schubert, C. Vogt, M. Woltmann, C. Lämmerzahl, S. Herrmann, W. Ertmer, E. M. Rasel, and D. Schlippert, Quantum test of the universality of free fall using rubidium and potassium, *The European Physical Journal D* **74**, 10.1140/epjd/e2020-10132-6 (2020).

[11] P. Asenbaum, C. Overstreet, M. Kim, J. Curti, and M. A. Kasevich, Atom-interferometric test of the equivalence principle at the  $10^{-12}$  level, *Phys. Rev. Lett.* **125**, 191101 (2020).

[12] M. Carlesso, S. Donadi, L. Ferrialdi, M. Paternostro, H. Ulbricht, and A. Bassi, Present status and future challenges of non-interferometric tests of collapse models, *Nature Physics* **18**, 243 (2022).

[13] T. Kovachy, P. Asenbaum, C. Overstreet, C. A. Donnelly, S. M. Dickerson, A. Sugarbaker, J. M. Hogan, and M. A. Kasevich, Quantum superposition at the half-metre scale, *Nature* **528**, 530 (2015).

[14] A. Bassi, K. Lochan, S. Satin, T. P. Singh, and H. Ulbricht, Models of wave-function collapse, underlying theories, and experimental tests, *Rev. Mod. Phys.* **85**, 471 (2013).

[15] B. Schrinski, P. Haslinger, J. Schmiedmayer, K. Hornberger, and S. Nimmrichter, Testing collapse models with bose-einstein-condensate interferometry, *Phys. Rev. A* **107**, 043320 (2023).

[16] G. Rosi, F. Sorrentino, L. Cacciapuoti, M. Prevedelli, and G. M. Tino, Precision measurement of the newtonian gravitational constant using cold atoms, *Nature* **510**, 518 (2014).

[17] R. H. Parker, C. Yu, W. Zhong, B. Estey, and H. Müller, Measurement of the fine-structure constant as a test of the standard model, *Science* **360**, 191 (2018).

[18] L. Morel, Z. Yao, P. Cladé, and S. Guellati-Khélifa, Determination of the fine-structure constant with an accuracy of 81 parts per trillion, *Nature* **588**, 61 (2020).

[19] T. L. Gustavson, P. Bouyer, and M. A. Kasevich, Precision rotation measurements with an atom interferometer gyroscope, *Physical Review Letters* **78**, 2046 (1997).

[20] B. Canuel, F. Leduc, D. Holleville, A. Gauguet, J. Fils, A. Virdis, A. Clairon, N. Dimarcq, C. J. Bordé, A. Landragin, and P. Bouyer, Six-axis inertial sensor using cold-atom interferometry, *Phys. Rev. Lett.* **97**, 010402 (2006).

[21] S. M. Dickerson, J. M. Hogan, A. Sugarbaker, D. M. S. Johnson, and M. A. Kasevich, Multiaxis inertial sensing with long-time point source atom interferometry, *Phys. Rev. Lett.* **111**, 083001 (2013).

[22] I. Dutta, D. Savoie, B. Fang, B. Venon, C. Garrido Alzar, R. Geiger, and A. Landragin, Continuous cold-atom inertial sensor with 1 nrad/sec rotation stability, *Phys. Rev. Lett.* **116**, 183003 (2016).

[23] D. Savoie, M. Altorio, B. Fang, L. A. Sidorenkov, R. Geiger, and A. Landragin, Interleaved atom interferometry for high-sensitivity inertial measurements, *Science advances* **4**, eaau7948 (2018).

[24] M. Anderson, J. Ensher, M. Matthews, C. Wieman, and E. Cornell, Observation of Bose-Einstein Condensation in a Dilute Atomic Vapor, *Science* **269**, 198 (1995).

[25] K. B. Davis, M.-O. Mewes, M. A. Joffe, M. R. Andrews, and W. Ketterle, Evaporative cooling of sodium atoms, *Physical Review Letters* **74**, 5202 (1995).

[26] T. Hensel, S. Loriani, C. Schubert, F. Fitzek, S. Abend, H. Ahlers, J.-N. Siemß, K. Hammerer, E. M. Rasel, and N. Gaaloul, Inertial sensing with quantum gases: a comparative performance study of condensed versus thermal sources for atom interferometry, *The European Physical Journal D* **75**, 10.1140/epjd/s10053-021-00069-9 (2021).

[27] D. Schlippert, C. Meiners, R. Rengelink, C. Schubert, D. Tell, É. Wodey, K. Zipfel, W. Ertmer, and E. Rasel, Matter-wave interferometry for inertial sensing and tests of fundamental physics, in *CPT and Lorentz Symmetry* (WORLD SCIENTIFIC, 2021).

[28] D. N. Aguilera, H. Ahlers, B. Battelier, A. Bawamia, A. Bertoldi, R. Bondarescu, K. Bongs, P. Bouyer, C. Braxmaier, L. Cacciapuoti, C. Chaloner, M. Chwalla, W. Ertmer, M. Franz, N. Gaaloul, M. Gehler, D. Gerardi, L. Gesa, N. Gürlebeck, J. Hartwig, M. Hauth, O. Hellmig, W. Herr, S. Herrmann, A. Heske, A. Hinton, P. Ireland, P. Jetzer, U. Johann, M. Krutzik, A. Kubelka, C. Lämmerzahl, A. Landragin, I. Lloro, D. Massonet, I. Mateos, A. Milke, M. Nofrarias, M. Oswald, A. Peters, K. Posso-Trujillo, E. Rasel, E. Rocco, A. Roura, J. Rudolph, W. Schleich, C. Schubert, T. Schultdt, S. Seidel, K. Sengstock, C. F. Sopuerta, F. Sorrentino, D. Summers, G. M. Tino, C. Trenkel, N. Uzunoglu, W. von Klitzing, R. Walser, T. Wendrich, A. Wenzlawski, P. Weßels, A. Wicht, E. Wille, M. Williams, P. Windpassinger, and N. Zahzam, Ste-quest—test of the universality of free fall using cold atom interferometry, *Classical and Quantum Gravity* **31**, 115010 (2014).

[29] A. Trimeche, B. Battelier, D. Becker, A. Bertoldi, P. Bouyer, C. Braxmaier, E. Charron, R. Corgier, M. Cornelius, K. Douch, N. Gaaloul, S. Herrmann, J. Müller, E. Rasel, C. Schubert, H. Wu, and F. Pereira dos Santos, Concept study and preliminary design of a cold atom interferometer for space gravity gradiometry, *Classical and Quantum Gravity* **36**, 215004 (2019).

[30] S. Loriani, D. Schlippert, C. Schubert, S. Abend, H. Ahlers, W. Ertmer, J. Rudolph, J. M. Hogan, M. A. Kasevich, E. M. Rasel, and N. Gaaloul, Atomic source selection in space-borne gravitational wave detection, *New Journal of Physics* **21**, 063030 (2019).

[31] A. E. Leanhardt, T. A. Pasquini, M. Saba, A. Schirotzek, Y. Shin, D. Kielpinski, D. E. Pritchard, and W. Ketterle, Cooling bose-einstein condensates below 500 picokelvin, *Science (New York, N.Y.)* **301**, 1513 (2003).

[32] P. Medley, D. M. Weld, H. Miyake, D. E. Pritchard, and W. Ketterle, Spin gradient demagnetization cooling of ultracold atoms, *Phys. Rev. Lett.* **106**, 195301 (2011).

[33] H. Ammann and N. Christensen, Delta kick cooling: A new method for cooling atoms, *Phys. Rev. Lett.* **78**, 2088 (1997).

[34] C. Deppner, W. Herr, M. Cornelius, P. Stromberger, T. Sternke, C. Grzeschik, A. Grote, J. Rudolph, S. Herrmann, M. Krutzik, A. Wenzlawski, R. Corgier, E. Charron, D. Guéry-Odelin, N. Gaaloul, C. Lämmerzahl, A. Peters, P. Windpassinger, and E. M. Rasel, Collective-mode enhanced matter-wave optics, *Phys. Rev. Lett.* **127**, 100401 (2021).

[35] N. Gaaloul, M. Meister, R. Corgier, A. Pichery, P. Boegel, W. Herr, H. Ahlers, E. Charron, J. R. Williams, R. J. Thompson, W. P. Schleich, E. M. Rasel, and N. P. Bigelow, A space-based quantum gas laboratory at picokelvin energy scales, *Nature communications* **13**, 7889 (2022).

[36] T. Kovachy, J. M. Hogan, A. Sugarbaker, S. M. Dickerson, C. A. Donnelly, C. Overstreet, and M. A. Kasevich, Matter wave lensing to picokelvin temperatures, *Phys. Rev. Lett.* **114**, 143004 (2015).

[37] W. Ketterle, D. S. Durfee, and D. M. Stamper-Kurn, Making, probing and understanding bose-einstein condensates (1999), arXiv:cond-mat/9904034 [cond-mat].

[38] S. Inouye, M. R. Andrews, J. Stenger, H.-J. Miesner, D. M. Stamper-Kurn, and W. Ketterle, Observation of feshbach resonances in a bose-einstein condensate, *Nature* **392**, 151 (1998).

[39] L. Masi, T. Petrucciani, A. Burchianti, C. Fort, M. Inguscio, L. Marconi, G. Modugno, N. Preti, D. Trypogeorgos, M. Fattori, and F. Minardi, Multimode trapped interferometer with noninteracting bose-einstein condensates, *Phys. Rev. Research* **3**, 043188 (2021).

[40] H. Albers, R. Corgier, A. Herbst, A. Rajagopalan, C. Schubert, C. Vogt, M. Woltmann, C. Lämmerzahl, S. Herrmann, E. Charron, W. Ertmer, E. M. Rasel, N. Gaaloul, and D. Schlippert, All-optical matter-wave lens using time-averaged potentials, *Communications Physics* **5**, 60 (2022).

[41] R. Roy, A. Green, R. Bowler, and S. Gupta, Rapid cooling to quantum degeneracy in dynamically shaped atom traps, *Phys. Rev. A* **93**, 043403 (2016).

[42] D. S. Jin, J. R. Ensher, M. R. Matthews, C. E. Wieman, and E. A. Cornell, Collective excitations of a bose-einstein condensate in a dilute gas, *Phys. Rev. Lett.* **77**, 420 (1996).

[43] M.-O. Mewes, M. R. Andrews, N. J. van Druten, D. M. Kurn, D. S. Durfee, C. G. Townsend, and W. Ketterle, Collective excitations of a bose-einstein condensate in a magnetic trap, *Phys. Rev. Lett.* **77**, 988 (1996).

[44] M. Egorov, B. Opanchuk, P. Drummond, B. V. Hall, P. Hannaford, and A. I. Sidorov, Measurement of *s*-wave scattering lengths in a two-component bose-einstein condensate, *Phys. Rev. A* **87**, 053614 (2013).

[45] J. M. Hogan, D. M. S. Johnson, S. Dickerson, T. Kovachy, A. Sugarbaker, S.-w. Chiow, P. W. Graham, M. A. Kasevich, B. Saif, S. Rajendran, P. Bouyer, B. D. Seery, L. Feinberg, and R. Keski-Kuha, An atomic gravitational wave interferometric sensor in low earth orbit (agis-leo), *General Relativity and Gravitation* **43**, 1953 (2011).

[46] B. Canuel, A. Bertoldi, L. Amand, E. Di Pozzo Borgo, T. Chantrait, C. Danquigny, M. Dovale Álvarez, B. Fang, A. Freise, R. Geiger, J. Gillot, S. Henry, J. Hinderer, D. Holleville, J. Junca, G. Lefèvre, M. Merzougui, N. Mielec, T. Monfret, S. Pelisson, M. Prevedelli, S. Reynaud, I. Riou, Y. Rogister, S. Rosat, E. Cormier, A. Landragin, W. Chaibi, S. Gaffet, and P. Bouyer, Exploring gravity with the miga large scale atom interferometer, *Scientific reports* **8**, 14064 (2018).

[47] M.-S. Zhan *et al.*, ZAIGA: Zhaoshan Long-baseline Atom Interferometer Gravitation Antenna, *Int. J. Mod. Phys. D* **29**, 1940005 (2019), arXiv:1903.09288 [physics.atom-ph].

[48] C. Schubert, D. Schlippert, S. Abend, E. Giese, A. Roura, W. P. Schleich, W. Ertmer, and E. M. Rasel, Scalable, symmetric atom interferometer for infrasound gravitational wave detection (2019), arXiv:1909.01951 [quant-ph].

[49] B. Canuel, S. Abend, P. Amaro-Seoane, F. Badaracco, Q. Beaufils, A. Bertoldi, K. Bongs, P. Bouyer, C. Braxmaier, W. Chaibi, N. Christensen, F. Fitzek, G. Flouris, N. Gaaloul, S. Gaffet, C. L. G. Alzar, R. Geiger, S. Guellati-Khelifa, K. Hammerer, J. Harms, J. Hinderer, M. Holynski, J. Junca, S. Katsanevas, C. Klemp, C. Kozanitis, M. Krutzik, A. Landragin, I. L. Roche, B. Leykauf, Y.-H. Lien, S. Loriani, S. Merlet, M. Merzougui, M. Nofrarias, P. Papadakos, F. P. dos Santos, A. Peters, D. Plexousakis, M. Prevedelli, E. M. Rasel, Y. Rogister, S. Rosat, A. Roura, D. O. Sabulsky, V. Schkolnik, D. Schlippert, C. Schubert, L. Sidorenkov, J.-N. Siemß, C. F. Sopuerta, F. Sorrentino, C. Struckmann, G. M. Tino, G. Tsagkatakis, A. Viceré, W. von Klitzing, L. Woerner, and X. Zou, Elgar—a european laboratory for gravitation and atom-interferometric research, *Classical and Quantum Gravity* **37**, 225017 (2020).

[50] L. Badurina, E. Bentine, D. Blas, K. Bongs, D. Bortolotto, T. Bowcock, K. Bridges, W. Bowden, O. Buchmueller, C. Burrage, J. Coleman, G. Elertas, J. Ellis, C. Foot, V. Gibson, M. Haehnelt, T. Harte, S. Hedges, R. Hobson, M. Holynski, T. Jones, M. Langlois, S. Lelouch, M. Lewicki, R. Maiolino, P. Majewski, S. Malik, J. March-Russell, C. McCabe, D. Newbold, B. Sauer, U. Schneider, I. Shipsey, Y. Singh, M. Uchida, T. Valenzuela, M. van der Grinten, V. Vaskonen, J. Vossebeld, D. Weatherill, and I. Wilmut, Aion: an atom interferometer observatory and network, *Journal of Cosmology and Astroparticle Physics* **2020** (05), 011.

[51] H. Ahlers, L. Badurina, A. Bassi, B. Battelier, Q. Beaufils, K. Bongs, P. Bouyer, C. Braxmaier, O. Buchmueller, C. Burrage, J. Coleman, G. Elertas, J. Ellis, C. Foot, V. Gibson, M. Haehnelt, T. Harte, S. Hedges, R. Hobson, M. Holynski, T. Jones, M. Langlois, S. Lelouch, M. Lewicki, R. Maiolino, P. Majewski, S. Malik, J. March-Russell, C. McCabe, D. Newbold, B. Sauer, U. Schneider, I. Shipsey, Y. Singh, M. Uchida, T. Valenzuela, M. van der Grinten, V. Vaskonen, J. Vossebeld, D. Weatherill, and I. Wilmut, Aion: an atom interferometer observatory and network, *Journal of Cosmology and Astroparticle Physics* **2020** (05), 011.

mueller, M. Carlesso, E. Charron, M. L. Chiofalo, R. Corgier, S. Donadi, F. Droz, R. Ecoffet, J. Ellis, F. Estève, N. Gaaloul, D. Gerardi, E. Giese, J. Grosse, A. Hees, T. Hensel, W. Herr, P. Jetzer, G. Kleinsteenberg, C. Klemp, S. Lecomte, L. Lopes, S. Loriani, G. Métris, T. Martin, V. Martín, G. Müller, M. Nofrarias, F. P. D. Santos, E. M. Rasel, A. Robert, N. Saks, M. Salter, D. Schlippert, C. Schubert, T. Schuldt, C. F. Sopuerta, C. Struckmann, G. M. Tino, T. Valenzuela, W. von Klitzing, L. Wörner, P. Wolf, N. Yu, and M. Zelan, *Ste-quest: Space time explorer and quantum equivalence principle space test* (2022), arXiv:2211.15412 [physics.space-ph].

[52] Y. A. El-Neaj, C. Alpigiani, S. Amairi-Pyka, H. Araújo, A. Balaž, A. Bassi, L. Bathe-Peters, B. Battelier, A. Belić, E. Bentine, J. Bernabeu, A. Bertoldi, R. Birmingham, D. Blas, V. Bolpasi, K. Bongs, S. Bose, P. Bouyer, T. Bowcock, W. Bowden, O. Buchmueller, C. Burrage, X. Calmet, B. Canuel, L.-I. Caramete, A. Carroll, G. Cella, V. Charmandaris, S. Chattopadhyay, X. Chen, M. L. Chiofalo, J. Coleman, J. Cotter, Y. Cui, A. Derevianko, A. De Roeck, G. S. Djordjevic, P. Dornan, M. Doser, I. Drougkakis, J. Dunningham, I. Dutan, S. Easo, G. Elertas, J. Ellis, M. El Sawy, F. Fassi, D. Felea, C.-H. Feng, R. Flack, C. Foot, I. Fuentes, N. Gaaloul, A. Gauguet, R. Geiger, V. Gibson, G. Giudice, J. Goldwin, O. Grachov, P. W. Graham, D. Grasso, M. van der Grinten, M. Gündogan, M. G. Haehnelt, T. Harte, A. Hees, R. Hobson, J. Hogan, B. Holst, M. Holynski, M. Kasevich, B. J. Kavanagh, W. von Klitzing, T. Kovachy, B. Krikler, M. Krutzik, M. Lewicki, Y.-H. Lien, M. Liu, G. G. Luciano, A. Magnon, M. A. Mahmoud, S. Malik, C. McCabe, J. Mitchell, J. Pahl, D. Pal, S. Pandey, D. Papazoglou, M. Paternostro, B. Penning, A. Peters, M. Prevedelli, V. Puthiyaveettil, J. Quenby, E. Rasel, S. Ravenhall, J. Ringwood, A. Roura, D. Sabulsky, M. Sameed, B. Sauer, S. A. Schäffer, S. Schiller, V. Schkolnik, D. Schlippert, C. Schubert, H. R. Sfar, A. Shayeghi, I. Shipsey, C. Signorini, Y. Singh, M. Soares-Santos, F. Sorrentino, T. Sumner, K. Tassis, S. Tentindo, G. M. Tino, J. N. Tinsley, J. Unwin, T. Valenzuela, G. Vasilakis, V. Vaskonen, C. Vogt, A. Webber-Date, A. Wenzlawski, P. Windpassinger, M. Woltmann, E. Yazgan, M.-S. Zhan, X. Zou, and J. Zupan, *Aedge: Atomic experiment for dark matter and gravity exploration in space*, EPJ Quantum Technology **7**, 10.1140/epjqt/s40507-020-0080-0 (2020).

[53] Y. Du, C. Murgui, K. Pardo, Y. Wang, and K. M. Zurek, Atom interferometer tests of dark matter, Phys. Rev. D **106**, 095041 (2022).

[54] L. Badurina, V. Gibson, C. McCabe, and J. Mitchell, Ultralight dark matter searches at the sub-hz frontier with atom multigradiometry, Phys. Rev. D **107**, 055002 (2023).

[55] S. Chu, J. E. Bjorkholm, A. Ashkin, J. P. Gordon, and L. W. Hollberg, Proposal for optically cooling atoms to temperatures of the order of  $10^{-6}$  k, Optics Letters **11**, 73 (1986).

[56] T. Weber, J. Herbig, M. Mark, H.-C. Nägerl, and R. Grimm, Bose-einstein condensation of cesium, Science (New York, N.Y.) **299**, 232 (2003).

[57] T. Kraemer, J. Herbig, M. Mark, T. Weber, C. Chin, H.-C. Nägerl, and R. Grimm, Optimized production of a cesium bose-einstein condensate, Applied Physics B **79**, 1013 (2004).

[58] G. Roati, M. Zaccanti, C. D'Errico, J. Catani, M. Modugno, A. Simoni, M. Inguscio, and G. Modugno,  $^{39}\text{K}$  bose-einstein condensate with tunable interactions, Phys. Rev. Lett. **99**, 010403 (2007).

[59] R. Corgier, S. Amri, W. Herr, H. Ahlers, J. Rudolph, D. Guéry-Odelin, E. M. Rasel, E. Charron, and N. Gaaloul, Fast manipulation of bose-einstein condensates with an atom chip, New J. Phys. **20**, 055002 (2018).

[60] S. Kirkpatrick, C. D. Gelatt, and M. P. Vecchi, Optimization by simulated annealing, Science **220**, 671 (1983).

[61] A. Herbst, T. Estrampes, H. Albers, V. Vollenkemper, K. Stolzenberg, S. Bode, E. Charron, E. M. Rasel, N. Gaaloul, and D. Schlippert, Creating nearly heisenberg-limited matter-waves exploiting tunable interactions (2023), arXiv:2307.06766 [cond-mat.quant-gas].

[62] J. Catani, P. Maioli, L. De Sarlo, F. Minardi, and M. Inguscio, Intense slow beams of bosonic potassium isotopes, Phys. Rev. A **73**, 033415 (2006).

[63] A. Herbst, H. Albers, K. Stolzenberg, S. Bode, and D. Schlippert, Rapid generation of all-optical  $^{39}\text{K}$  bose-einstein condensates using a low-field feshbach resonance, Phys. Rev. A **106**, 043320 (2022).

[64] H. Albers, *Time-averaged optical potentials for creating and shaping Bose-Einstein condensates*, Ph.D. thesis, Leibniz Universität Hannover (2020).

[65] G. Salomon, L. Fouché, P. Wang, A. Aspect, P. Bouyer, and T. Bourdel, Gray-molasses cooling of  $^{39}\text{K}$  to a high phase-space density, EPL (Europhysics Letters) **104**, 63002 (2013).

[66] C. D'Errico, M. Zaccanti, M. Fattori, G. Roati, M. Inguscio, G. Modugno, and A. Simoni, Feshbach resonances in ultracold  $^{39}\text{K}$ , New Journal of Physics **9**, 223 (2007).

[67] M. Landini, S. Roy, G. Roati, A. Simoni, M. Inguscio, G. Modugno, and M. Fattori, Direct evaporative cooling of  $^{39}\text{K}$  atoms to bose-einstein condensation, Phys. Rev. A **86**, 033421 (2012).

[68] R. Corgier, S. Loriani, H. Ahlers, K. Posso-Trujillo, C. Schubert, E. M. Rasel, E. Charron, and N. Gaaloul, Interacting quantum mixtures for precision atom interferometry, New Journal of Physics **22**, 123008 (2020).

[69] Y. Castin and R. Dum, Bose-einstein condensates in time dependent traps, Physical Review Letters **77**, 5315 (1996).

[70] Y. Kagan, E. L. Surkov, and G. V. Shlyapnikov, Evolution of a bose gas in anisotropic time-dependent traps, Phys. Rev. A **55**, R18 (1997).

[71] C. J. Pethick and H. Smith, *Bose-Einstein Condensation in Dilute Gases*, 2nd ed. (Cambridge University Press, 2008).

[72] V. M. Pérez-García, H. Michinel, J. I. Cirac, M. Lewenstein, and P. Zoller, Low energy excitations of a bose-einstein condensate: A time-dependent variational analysis, Phys. Rev. Lett. **77**, 5320 (1996).

[73] V. M. Pérez-García, H. Michinel, J. I. Cirac, M. Lewenstein, and P. Zoller, Dynamics of bose-einstein condensates: Variational solutions of the gross-pitaevskii equations, Phys. Rev. A **56**, 1424 (1997).

## ACKNOWLEDGEMENTS

We thank Dorothee Tell for thorough proof reading. This work is funded by the German Space

Agency (DLR) with funds provided by the Federal Ministry for Economic Affairs and Climate Action due to an enactment of the German Bundestag under Grant No. DLR 50WM2041 (PRIMUS-IV), 50WM2253A (AI-Quadrat) and supported by the “ADI 2022” project founded by the IDEX Paris-Saclay, ANR-11-IDEX-0003-02. The authors further acknowledge support by the Federal Ministry of Education and Research (BMBF) through the funding program Photonics Research Germany under contract number 13N14875 and by the Deutsche Forschungsgemeinschaft (DFG, German Research Foundation)—Project-ID 274200144—the SFB 1227 DQ-mat within Project No. A05 and B07 and under Germany’s Excellence Strategy—EXC-2123 QuantumFrontiers—Project-ID 390837967.

#### AUTHOR CONTRIBUTIONS

A.H., H.A., S.B., E.M.R. and D.S. designed the experimental setup and the dipole trapping laser system. A.H.,

H.A., S.B., K.S., E.M.R. and D.S. contributed to the design, operation, and maintenance of the overall setup. T.E., R.C., E.C. and N.G. set the theoretical framework of this work. A.H., T.E. and H.A. with support of R.C., E.C. and N.G. performed the analysis of the data presented in this manuscript. A.H., T.E. and R.C. with support of D.S., E.C., E.M.R. and N.G. drafted the initial manuscript. All authors discussed and evaluated the results and contributed to, reviewed, and approved of the manuscript.

#### COMPETING INTERESTS

All authors declare no competing interests.